Journal of Science and Technology – Smart Systems and Devices
Volume x, Issue x, Month Year, ppp–ppp

Dynamic Analysis of a Two-Degree-of-Freedom Engine-Chassis System Using a Magnetorheological Mount

Tuan Hoang Quang, Cuong Do Van*
Hanoi University of Industry, Ha Noi, Vietnam
* *Corresponding author email: cuongdv@haui.edu.vn*

Abstract

This study presents the mathematical modeling and dynamic analysis of a two-degree-of-freedom (2DOF) engine-chassis system utilizing a magnetorheological (MR) mount integrated with a magnetic shield. Based on the Bingham plastic model, numerical simulations were conducted using the ODE45 solver in MATLAB/Simulink to quantitatively evaluate the vibration responses in both the time and frequency domains under varying excitation currents ranging from 0 to 2 A. The results indicate that the MR mount exhibits superior vibration attenuation capabilities; as the applied current increases, the displacement and velocity amplitudes of the engine are significantly reduced, particularly at the two resonance peaks of 1.07 Hz (in-phase) and 3.47 Hz (out-of-phase). However, the study reveals that excitation currents above 1.25 A are counterproductive to overall chassis ride comfort. This performance degradation at high currents is physically governed by the classical damping-transmissibility trade-off at frequencies well above resonance, leading to an observed increase in the chassis response. The optimal operating region is determined to be within the current range of 0 A to 1.0 A, where the acceleration amplitude transmitted to the chassis is maintained at a low level. This research not only solidifies the theoretical foundation for modeling smart mounting systems but also provides essential data for developing semi-active control strategies, thereby promoting the practical application potential of MR mounts in the automotive industry.

Keywords: Magnetic saturation, magnetorheological fluid (MR fluid), magnetorheological mount (MR mount), two-degree-of-freedom (2DOF), vibration isolation.

In press

1. Introduction

Vibration in automobiles mainly originates from engine oscillation due to intermittent combustion processes, inertial forces of moving components, and random excitations from road profiles. These vibrations are transmitted through the mounting system to the chassis, negatively affecting structural durability, operational stability, and NVH (Noise, Vibration, and Harshness) indices [1–4]. Traditional damping methods such as rubber or hydraulic mounts are passive in nature, featuring fixed stiffness and damping coefficients [5, 6]. Therefore, they face limitations in reconciling two conflicting requirements: high dynamic stiffness at low-frequency ranges (1-30 Hz) to restrict engine displacement, and low stiffness at high-frequency ranges (30-250 Hz) to isolate vibrations and prevent structure-borne noise from entering the cabin [7].

To address this problem, the magnetorheological mount (MR mount) utilizing Magnetorheological fluid (MR fluid) has become a promising research trend [8]. Magnetorheological fluid is a smart material capable of changing its state from liquid to semi-solid within a few milliseconds when exposed to a magnetic field [5, 9]. The variation in the yield stress of the MR fluid is directly proportional to the excitation current intensity. This mechanism grants the MR mount system the ability to automatically tune damping forces and dynamic stiffness parameters in real-time to attenuate complex excitation frequency bands. Thanks to this flexible response capability, MR technology has been effectively applied in improving engine and cabin mounting systems to enhance vehicle vibration isolation quality [5, 10, 11]. However, the application of MR mounts in automobiles remains modest. Stemming from this gap, this study develops a magnetorheological mount structure using a magnetic shield that provides superior damping force, indicating strong potential for automotive application. Specifically, this research focuses on constructing a mathematical model and dynamically analyzing a two-degree-of-freedom (2DOF) engine-chassis system to quantitatively evaluate the vibration isolation effectiveness of the MR mount via numerical simulation methods.

2. Mathematical Model and Research Methodology

2.1. Damping Force Model of the MR Mount

The study inherits the magnetorheological mount configuration using a magnetic shielding ring, which the research group has previously investigated. This configuration exhibits outstanding damping characteristics due to the magnetic flux being directionally concentrated into the MR fluid layer [8]. Accordingly, the total damping force generated by the MR mount consists of three fundamental components:

p-ISSN 3093-3285
e-ISSN 3093-3315
https://doi.org/10.51316/jst.xxx.ssad.xxxx.xx.x.x
Received: Aug 28, 2026; Revised: Oct 14, 2026;
Accepted: Oct 16, 2026; Online: Nov 12, 2026

the elastic force of the rubber, the viscous damping force of the base fluid, and the yield force generated by the magnetic field effect. Based on the Bingham Plastic model for MR fluid flow, the total damping force Fd is described by the following equation [8]:

$$F_d = F_1 + F_\eta + F_\tau \quad (1)$$

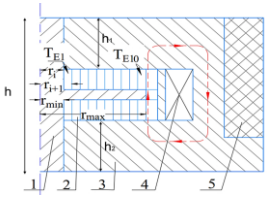
Where: $F_1 = k_{rubber}.(x - z)$ is the elastic force of the rubber (N), $F_\eta = C_{MR}(I).(\dot{x} - \dot{z})$ is the viscous damping force of the fluid (N), F_τ is the force generated by the magnetic field effect (N).

The damping force due to the magnetic field effect is calculated by integrating over the radius[1]:

$$F_\tau = \int_{r_{min}}^{r_{max}} \frac{2\tau_y}{h-x(t)}(r_{max} - r)2\pi r dr$$

$$= \frac{4\pi\tau_y}{h-x(t)}\left(\frac{r_{max}({r_{max}}^2 - {r_{min}}^2)}{2} - \frac{{r_{max}}^3 - {r_{min}}^3}{3}\right) \quad (2)$$

In practice, the magnetic field strength is non-uniformly distributed along the radius, therefore the yield stress also varies radially (r). For a more accurate calculation, the disk surface is divided into 10 concentric circular zones, each with an inner radius r_i and an outer radius r_{i+1}, as illustrated in Fig. 1.



1: Disc-Steel 2: MR Fluid 3: Housing
4: Coil 5: Rubber

Fig. 1. Structure of the MR mount [1]

In each zone, assuming that the yield stress $\tau_{y,i}(H)$ is constant, the force induced by the magnetic field in the *i-th* zone is approximated by [1]:

$$F_{\tau,i} = \int_{r_i}^{r_{i+1}} \frac{2\tau_{yi}}{h - x(t)}(r_{max} - r).2\pi r dr$$

$$= \frac{4\pi\tau_{yi}}{h-x(t)}.\left(\frac{r_{max}({r_{i+1}}^2 - {r_i}^2)}{2} - \frac{{r_{i+1}}^3 - {r_i}^3}{3}\right) \quad (3)$$

The total magnetic force acting on the entire disk is [1]:

$$F_\tau = \sum_{i=1}^{10} F_{\tau,i} \quad (4)$$

Considering the characteristics of axial translational motion and the operating mechanism of the MR fluid, only the gap under compression generates a force due to the magnetic field effect. Therefore, the generated force depends on the direction of the velocity.[1].

$$F_\tau = \begin{cases} \frac{4\pi\tau_y}{h_1 - x(t)}.\left(\frac{r_{max}({r_{max}}^2 - {r_{min}}^2)}{2} - \frac{{r_{max}}^3 - {r_{min}}^3}{3}\right), & \dot{x} - \dot{z} > 0 \\ \frac{4\pi\tau_y}{h_2 + x(t)}.\left(\frac{r_{max}({r_{max}}^2 - {r_{min}}^2)}{2} - \frac{{r_{max}}^3 - {r_{min}}^3}{3}\right), & \dot{x} - \dot{z} < 0 \end{cases} \quad (5)$$

Since the MR mount is installed between the engine and the chassis, its damping force acts to oppose the relative motion across the mount. Therefore, the direction of the magnetorheological force F_τ is governed by the sign of the relative velocity $\dot{x} - \dot{z}$. This relative velocity formulation was consistently used in both the mathematical modeling and the Simulink implementation.

2.2. Dynamic Equations of The Two-Degree-of-Freedom System

To focus on evaluating the vertical vibration isolation capability (Z-axis), the system is modeled as a 2DOF vibration system comprising the engine mass (m_e) and the sprung mass/chassis mass (m_c). The MR Mount is placed between the engine and the chassis, while the vehicle suspension system is characterized by stiffness k and damping coefficient c.

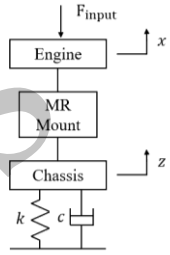


Fig. 2. 2DOF model using MR mount

The differential equations of motion for the system under the forced excitation F_{input} from the engine are established based on the dynamic equilibrium principle (D'Alembert's principle) as follows:

$$m_e\ddot{x} + C_{MR}(I).(\dot{x} - \dot{z}) + k_{rubber}(x - z) + F_\tau(\dot{x} - \dot{z}) = F_{input}$$

$$m_c.\ddot{z} + k.z + C_s.\dot{z} - C_{MR}(I).(\dot{x} - \dot{z}) - k_{rubber}(x - z) - F_\tau(\dot{x} - \dot{z}) = 0 \quad (6)$$

Solving the system of equations (6) in the MATLAB/Simulink environment extracts the responses in the time domain and frequency domain (Fig. 3).

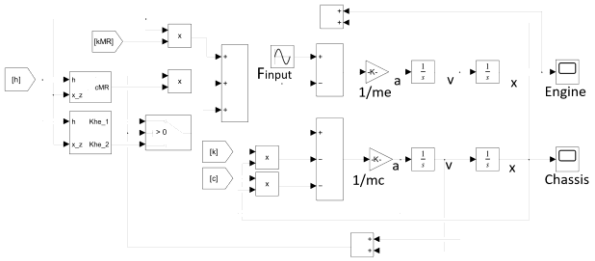


Fig. 3. Simulink simulation model for the 2DOF engine-chassis system

The simulation parameters are selected closely following actual operating conditions: m_e= 50 kg, m_c= 300 kg, k_{rubber} = 20000 N/m. The input parameters fed into the simulation are taken according to Table 1.

Inpress

Table 1. Input parameters for the 2DOF system

Parameter	Value
Engine mass 1/4 m_e (kg) [12]	50
Sprung mass m_c (kg) [12]	300
Rubber mount stiffness k_{rubber} (N/m) [12]	20000
Spring stiffness k (N/m) [13]	16000
MR fluid viscosity η (Pa.s) [14]	0.112
Investigation current I (A)	0-2 (step 0.25)
Forced excitation force F_{input} (N) [15]	100sin(ωt)
Damping of the suspension system C_s (N/m) [13]	1000

For the dynamic simulation, a 2DOF engine–chassis model was developed in MATLAB/Simulink. The governing differential equations were solved using the variable-step Dormand–Prince solver (ODE45), with a maximum time step of 0.001 s and a specified relative tolerance to ensure numerical stability and accuracy. The model accounts for the interactions between the engine, chassis, and MR mount force, and enables analysis of both time- and frequency-domain responses.

3. Simulation Results and Discussion

3.1. Dynamic Response Analysis in the Time Domain

3.1.1. Time-domain dynamic response of the engine block

Displacement response

Fig. 4 clearly shows the influence of the excitation current intensity on the engine displacement amplitude over time. When no current is applied (I = 0 A), the displacement amplitude reaches its maximum value, with the highest vibration peak reaching approximately 2.3 × 10^{-3} m in the first second and maintaining the highest vibration level throughout the 25-second investigation period.

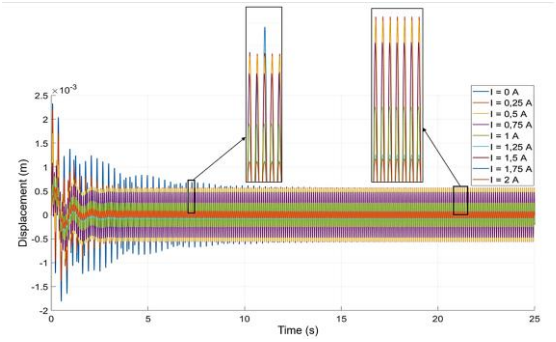


Fig. 4. Engine displacement response over time under the influence of various excitation currents (0-2A)

However, when the current intensity is gradually increased to 0.25 A, 0.5 A, 0.75 A, and 1 A, the displacement amplitude decreases significantly. At the maximum current I = 2 A, the vibration amplitude drops to its minimum, reaching just under 0.5 × 10^{-3} m. This result shows that increasing the control current for the MR mount significantly enhances the ability to attenuate vibration and control engine displacement. Furthermore, the vibration reduction effectiveness tends to saturate from a current level of 1.25 A onwards, as the response curves lie very close to each other.

Velocity response

Fig. 5 illustrates the vibration velocity response of the engine over time under the effect of different excitation currents. Without current (0 A), the velocity amplitude reaches its maximum, fluctuating strongly at approximately ±0.06 m/s during the initial transient phase and remaining at the highest level throughout the process. However, as the current intensity gradually increases, the velocity amplitude decreases markedly. Specifically, at current levels from 0.5 A to 1.25 A, the damping force from the mounting system exerts a highly effective energy dissipation effect, strongly suppressing the vibration velocity.

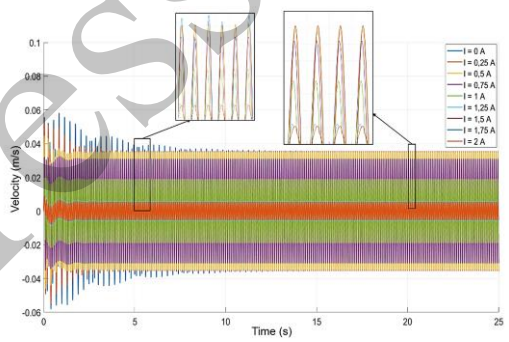


Fig. 5. Engine velocity response over time under the influence of various excitation currents (0-2A)

Furthermore, as the current continues to increase from 1.25 A to the maximum of 2 A, the velocity amplitude enters a saturation state, narrowing to a very small level (under ±0.01 m/s) with almost no further reduction. Thus, it can be seen that increasing the current beyond the 1.25 A threshold is redundant and provides no additional vibration isolation benefits.

3.1.2. Time-domain dynamic response of the chassis

Chassis displacement response

Fig. 6 represents the chassis displacement response over time under control currents from 0 A to 2 A. During the initial transient phase, the vibration amplitude exhibits a high overshoot, peaking at approximately 8 × 10^{-4} m before rapidly declining. However, when the system enters a stable vibration state (from the 10th second onwards), the response trend of the chassis displays a complete contrast compared to the engine block.

Specifically, at I = 0 A, the chassis vibration amplitude is maintained at the minimum value.

Express

Conversely, as the current intensity continuously increases to 1.75 A and 2 A, the stiffness of the MR mount rises sharply, causing it to transmit a large amount of vibration directly to the undercarriage, raising the chassis displacement to its highest level. This result proves that applying excessive current beyond the saturation threshold is counterproductive and severely degrades the vehicle's ride comfort.

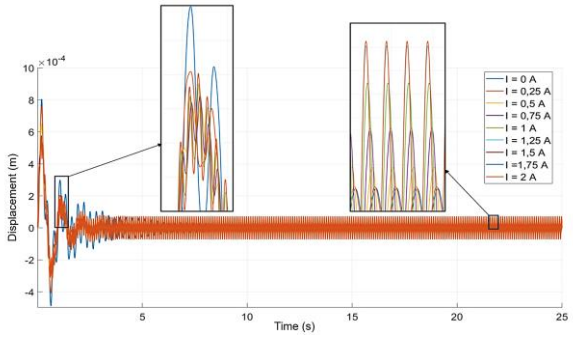


Fig. 6. Chassis displacement response over time under the influence of various excitation currents (0-2A)

Chassis velocity response

Fig. 7 illustrates the chassis vibration velocity response over time under control current from 0 A to 2 A. In the initial transient stage, the vibration velocity fluctuates wildly, reaching a peak of approximately 0.02 m/s before beginning to decline. However, when the system enters the steady state, the difference between the current levels becomes evident. Specifically, at 0 A, the chassis vibration velocity amplitude is kept to a minimum. On the contrary, when the current intensity continuously increases to 1.75 A and 2 A, the MR mount significantly stiffens, transmitting vibrations directly to the chassis and pushing the chassis velocity amplitude to its highest level (about ±0.0075 m/s). This result affirms that supplying excessive current beyond the saturation threshold will reduce the vehicle's overall vibration isolation performance.

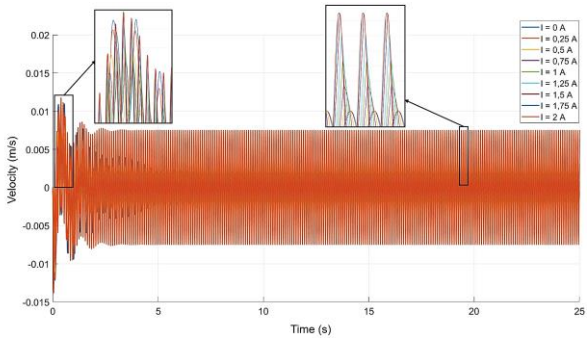


Fig. 7. Chassis velocity response over time under the influence of various excitation currents (0-2A)

3.1.3. Acceleration of the engine and chassis engine acceleration

Fig. 8 shows the engine acceleration response over time under excitation current from 0 A to 2 A. The continuous vibrations form a dense band with a large amplitude in the range of approximately ±2.8 m/s². However, in the magnified chart area, the differentiation between current levels is very clear. Specifically, when no current is applied (0 A), the acceleration amplitude peaks.

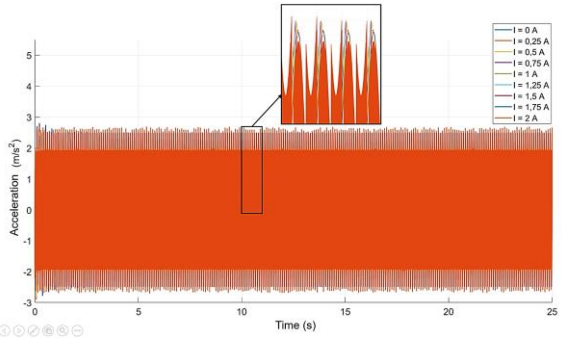


Fig. 8. Engine acceleration response over time under the influence of various excitation currents (0-2A)

Conversely, as the current intensity gradually increases to 1 A and 1.25 A, the acceleration amplitude drops sharply due to the greater damping force generated by the MR mount. Additionally, as the current continues to increase to 1.75 A and 2 A, the engine acceleration barely decreases further, entering a saturation state at the lowest amplitude level (about ±2.0 m/s²). This result confirms that the system has reached its magnetic saturation limit; hence, supplying excess current will not yield further vibration isolation efficiency.

Chassis acceleration

Fig. 9 presents the chassis acceleration response over time under the influence of control currents from 0 A to 2 A. Specifically, in the low-current ranges (from 0 A to 1 A), the MR mount operates effectively, helping to maintain the chassis acceleration amplitude at a low and stable level, fluctuating steadily around ±0.45 m/s².

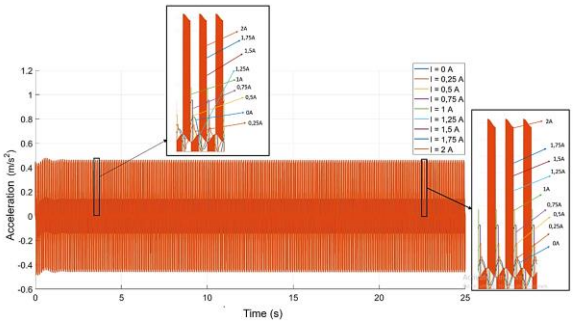


Fig. 9. Chassis acceleration response over time under the influence of various excitation currents (0-2A)

However, when the current intensity exceeds the 1.25 A threshold, especially at the 1.75 A and 2 A levels, the system falls into a "stiffening" state due to magnetic saturation. As a result, the MR Mount transmits harsh vibrations directly to the undercarriage, causing the acceleration amplitude to spike with sharp pulse peaks

In press

reaching the 1.2 m/s² threshold (clearly shown in the two magnified frames). In summary, continuing to supply currents greater than 1.25 A not only fails to provide damping benefits but also seriously disrupts the vehicle's ride comfort criteria.

3.2. Dynamic Response Analysis in the Frequency Domain

Fig. 10 illustrates the displacement responses of the engine block and chassis in the frequency domain when no control current is applied (0 A). In general, the 2DOF vibration system exhibits two resonance states. Specifically, at the low-frequency range (around 1 Hz), both the engine and the chassis share a common resonance peak where the displacement amplitude jumps to its maximum, reaching approximately 22 mm and 16.5 mm, respectively. However, as the excitation frequency progresses to around 3.5 Hz, a second resonance peak (out-of-phase resonance) continues to appear clearly in the engine assembly, with the amplitude rising to 5.5 mm; meanwhile, the chassis displacement at this frequency drops sharply without forming a peak. Furthermore, as the frequency continues to exceed 10 Hz, the vibration of the entire system gradually enters a stable forced state, causing the displacement amplitudes of both the engine and chassis to rapidly approach 0 mm.

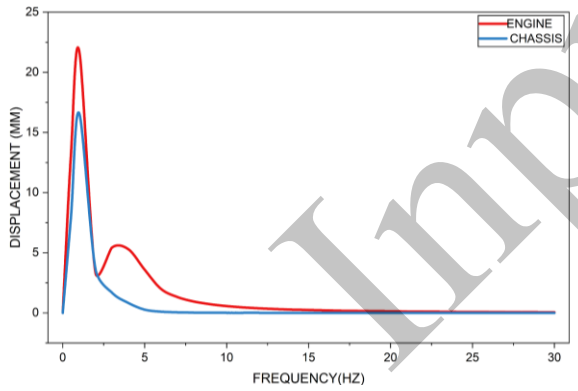


Fig. 10. Engine and chassis displacement response in the frequency domain with no excitation current (0 A)

The 3D graph in Fig. 11 presents the engine displacement response in the frequency domain under control currents from 0 A to 2 A. Specifically, in the low-frequency region (from 1 Hz to 5 Hz), the system exhibits a pronounced resonance phenomenon. When no current is applied (0 A), the displacement amplitude spikes to its maximum, reaching approximately 21.9 mm. However, as the current intensity gradually increases, the amplitude at the first resonance peak significantly diminishes thanks to the increase in the mount's magnetic damping force. Concurrently, the second resonance peak is also flattened and almost entirely disappears at high current levels. Furthermore, when the excitation frequency exceeds 10 Hz, the vibration amplitude is quickly suppressed and approaches 0 mm regardless of the current intensity. In conclusion, these quantitative results demonstrate the MR mount system's excellent ability to control resonance and attenuate vibration.

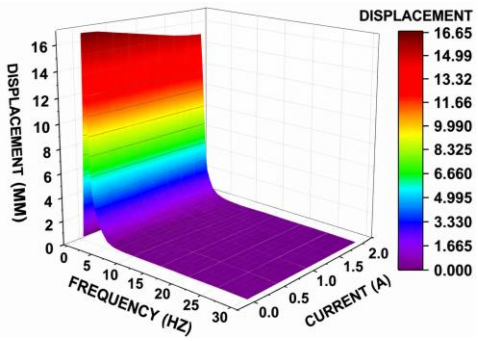


Fig. 11. 3D chart of engine displacement response in the frequency domain under the influence of various excitation currents (0 - 2 A)

The 3D graph in Fig. 12 illustrates the chassis displacement response in the frequency domain under current levels from 0 A to 2 A. Specifically, the vibration is predominantly concentrated in the low-frequency band, creating the largest resonance peak of approximately 16.65 mm at around 1 Hz when no current is applied (0 A).

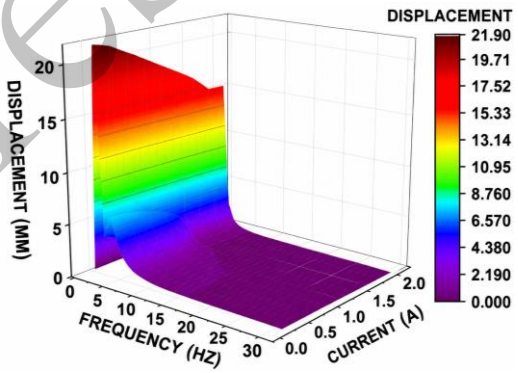


Fig. 12. 3D chart of chassis displacement response in the frequency domain under the influence of various excitation currents (0 - 2 A)

However, as the excitation current intensity gradually increases, this resonance amplitude declines due to the enhanced damping force of the MR Mount. On the other hand, once the excitation frequency surpasses the 5 Hz threshold, the displacement amplitude plummets immediately. Especially in the frequency range from 10 Hz to 30 Hz, the chassis vibration is almost completely eliminated, approaching 0 mm regardless of changes in the control current. Therefore, this quantitative result affirms the MR mount's absolute vibration isolation capability for the chassis segment at high-frequency ranges.

4. CONCLUSION

Based on the 2DOF mathematical model and numerical simulation results in the MATLAB/Simulink environment, this study comprehensively evaluated the

Inpress

dynamics of an engine-chassis system utilizing a magnetorheological mount (MR Mount). The conclusions drawn from the research include:

- The study successfully established a 2DOF dynamic model incorporating the Bingham plastic flow model for the magnetorheological mount. The application of the magnetic shield configuration demonstrated a significant increase in generating concentrated damping force, proving the mechanism's flexibility in adjusting stiffness and damping coefficients.

- In both the time and frequency domains, the MR Mount exhibits outstanding vibration energy suppression capabilities. At low-frequency ranges, increasing the excitation current significantly lowers the amplitudes at the two resonance peaks (in-phase vibration at 1 Hz and out-of-phase at 3.5 Hz), protecting the engine structure from hazardous vibrations.

- The study clearly identified the optimal operating region of the system as the current range from 0 A to 1.0 A. Within this region, the mount maintains the acceleration amplitude transmitted to the chassis at a low level, ensuring ride comfort. At currents above 1.25 A, an increase in the chassis response was observed within the investigated current range. This indicates that excessively increasing the excitation current may adversely affect the vehicle's dynamic performance.

- However, because the current study is limited to numerical simulation methods, future development directions will focus on manufacturing a prototype and conducting experimental measurements to comprehensively validate the model's reliability.

In conclusion, the research results provide a solid scientific foundation and practical design guidelines for applying smart damping technology in automobiles. Subsequent developments can focus on integrating control algorithms to automatically fine-tune the current according to the vehicle's actual operating conditions.

Acknowledgments

This work was supported by Hanoi University of Industry, Vietnam under the science, technology and innovation project, grant number 02/2026-NVTN.

References

[1] J. Fu, C. Huang, R. Shu, X. Quan, M. Chen, Z. Chen, and B. Chen, Multi-objective optimization of magnetorheological mount considering optimal damping force and maximum adjustable coefficient, Machines, vol. 11, no. 1, p. 60, Jan. 2023. https://doi.org/10.3390/machines11010060

[2] W. Lv, K. Chen, W. Li, and M. Dong, A Method for analysing in-vehicle acoustic response to engine excitation, Engineering, vol. 6, no. 11, p. 285, Oct. 2025. https://doi.org/10.3390/eng6110285

[3] Z. Rao, L. Tang, and Y. Shi, Structural design and static stiffness optimization of magnetorheological suspension for automotive engine, Applied Sciences, vol. 14, no. 16, Aug. 2024, Art. no. 6975. https://doi.org/10.3390/app14166975

[4] Q. Liu, G.-D. Bai, Z.-H. Liu, X.-X. F. Bai, H. Du. P. Chen, and L.-J. Qian, Magnetorheological semi-active mount system for engines: prototyping and testing, Proceedings of the Institution of Mechanical Engineers, Part D: Journal of Automobile Engineering, vol. 234, iss. 13, pp. 3081–3094, Jun. 2020. https://doi.org/10.1177/0954407020925724

[5] S.-Y. Yang, C. Han, S.-U. Shin, and S.-B. Choi, Design and evaluation of a semi-active magneto-rheological mount for a wheel loader cabin, Actuators, vol. 6, no. 2, p. 16, Apr. 2017. https://doi.org/10.3390/act6020016

[6] R. N. Jazar, Vehicle Dynamics: Theory and Application, Cham, Switzerland: Springer Nature, 2025.

[7] H. Q. Tuan and N. M. Dung, Analysis of the damping performance of an automotive seat suspension system using a magnetorheological mount via an integrated simulation approach, HaUI Journal of Science and Technology, vol. 62, no. 6A, pp. 207–213, Jun. 2026, (In Vietnamese: Phân tích hiệu quả giảm chấn của hệ thống treo ghế ô tô bằng gối đỡ từ lưu biến thông qua phương pháp mô phỏng tích hợp). https://doi.org/10.57001/huih5804.2026.168

[8] J. S. Kumar, P. S. Paul, G. Raghunathan, and D. G. Alex, A review of challenges and solutions in the preparation and use of magnetorheological fluids, International Journal of Mechanical and Materials Engineering, vol. 14, no. 1, Nov. 2019, Art. no. 13. https://doi.org/10.1186/s40712-019-0109-2

[9] Z. Deng, Q. Yang, and X. Yang, Optimal design and experimental evaluation of magneto-rheological mount applied to start/stop mode of vehicle powertrain, Journal of Intelligent Material Systems and Structures, vol. 31, iss. 8, pp. 1126–1137, May 2020. https://doi.org/10.1177/1045389X20910271

[10] S.-H. Kim, D.-S. Yoo, G.-W. Kim, S.-B. Choi, J.-Y. Jeong, J.-H. Kim, S.-J. Kim, and I.-D. Kim, Road traveling test for vibration control of a wheel loader cabin installed with magnetorheological mounts, Journal of Intelligent Material Systems and Structures, vol. 32, iss. 12, pp. 1336–1348, Jul. 2021. https://doi.org/10.1177/1045389X20953900

[11] Q. T. Hoang and H. Q. Vu, Parametric study on the magnetic circuit of MR mounts utilizing magnetic shielding, Scientific Journal of Silesian University of Technology. Series Transport, vol. 132, pp. 129–144, 2026. https://doi.org/10.20858/sjsutst.2026.132.7

[12] B. Sapiński and J. J. Snamina, Automotive vehicle engine mount based on an MR squeeze-mode damper: modeling and simulation, Journal of Theoretical and Applied Mechanics, vol. 55, no. 1, pp. 377–388, Jan. 2017.

[13] X. F. Bai, P. Chen, L.-J. Qian, and P. Kan, Design and analysis of a magnetorheological fluid mount featuring uni-directional squeeze mode, in Proceedings of the ASME 2015 Conference on Smart Materials, Adaptive Structures and Intelligent Systems (SMASIS2015),

In press

Colorado Springs, CO, USA, Sep. 2015, Paper No. SMASIS2015-8813.

[14] LORD Corporation, MRF-132DG Magneto-Rheological Fluid,. [Online]. Available: https://www.shoplordmr.com/mr-products/mrf-132dg-magneto-rheological-fluid-1-liter, Accessed on: Jul. 31, 2025.

[15] H. P. Salunkhe, S. Thikane, and S. Sadale, Magnetorheological damper and its applications: current scenario and future prospects, Romanian Journal of Acoustics and Vibration, vol. 20, no. 1, pp. 20–29, Aug. 2023.

Impress